

Multimodal Image-to-Image Translation via Mutual Information Estimation and Maximization

Zhiwen Zuo,¹ Qijiang Xu,² Huiming Zhang,¹ Zhizhong Wang,¹
Haibo Chen,¹ Ailin Li,¹ Lei Zhao,^{1*} Wei Xing,^{1†} Dongming Lu¹

¹ Zhejiang University ² Seattle AI Lab, Kwai Inc.

{zzwcs, qinglanwuji, endywon, feng123, liailin, cszhl, wxing, ldm}@zju.edu.cn, xuqijiang@kuaishou.com

Abstract

In this paper, we present a novel framework that can achieve multimodal image-to-image translation by simply encouraging the statistical dependence between the latent code and the output image in conditional generative adversarial networks. In addition, by incorporating a U-net generator into our framework, our method only needs to learn a one-sided translation model from the source image domain to the target image domain for both supervised and unsupervised multimodal image-to-image translation. Furthermore, our method also achieves disentanglement between the source domain content and the target domain style for free. We conduct experiments under supervised and unsupervised settings on various benchmark image-to-image translation datasets compared with the state-of-the-art methods, showing the effectiveness and simplicity of our method to achieve multimodal and high-quality results.

Introduction

In recent years, Generative Adversarial Networks (GANs) (Goodfellow et al. 2014) have emerged as a promising generative model that can capture complex and high-dimensional image data distributions. Extended on GANs, conditional GANs (cGANs) (Mirza and Osindero 2014) which take extra contextual information as input are widely used in conditional image synthesis and achieve great success, such as (Pathak et al. 2016; Isola et al. 2017; Ledig et al. 2017; Zhang et al. 2017), to name a few.

Image-to-image translation (I2IT) aims to map images in source domain to images in target domain while maintaining the underlying spatial information in the input image. As a central problem in computer vision, many conditional image synthesis problems can be seen as special cases of I2IT, for example, super resolution (Ledig et al. 2017), image inpainting (Pathak et al. 2016), and style transfer (Gatys, Ecker, and Bethge 2016). The problem is considered supervised or unsupervised according to whether paired images are available. Many pioneering works (Isola et al. 2017; Wang et al. 2018) on I2IT only learn a deterministic mapping function given paired data. Further, for the unpaired problem, cycle consistency (Zhu et al. 2017a; Kim et al. 2017; Yi et al. 2017)

is proposed to guarantee the maintenance of the underlying spatial information of the input image by mapping the translated images back to their inputs. Therefore, bidirectional mappings between the source image domain and the target image domain need to be learned simultaneously under an unsupervised setting. On the other hand, I2IT should be capable of producing multiple possible outputs even for a single input image, for example, a Yosemite winter photo may correspond to multiple summer photos that vary in light, the amount of clouds, and the luxuriance of vegetation. A straightforward way to produce diverse results for cGANs is to distill such variations in latent noise that can be sampled from a simple distribution, such as an isotropic Gaussian. However, it has been reported in the literature (Isola et al. 2017; Zhu et al. 2017b; Mathieu, Couprie, and LeCun 2015) that cGANs are prone to ignore the variation of the latent noise, which is also known as the issue of mode collapse (Goodfellow et al. 2014; Metz et al. 2016; Goodfellow 2016).

Many previous works (Zhu et al. 2017b; Lee et al. 2018; Huang et al. 2018; Almahairi et al. 2018) solve the diversity problem for supervised or unsupervised multimodal I2IT all by introducing encoders in their frameworks to learn a one-to-one mapping between the latent code space and the output image space via latent code reconstruction loss, which is in principle related to maximizing a variational lower bound on the mutual information between the latent code and the output image (Chen et al. 2016) in CGANs. Therefore, their success of achieving multimodal results can also in some extent be attributed to the implicit mutual information maximization. Among them, Huang et al. and Lee et al. further disentangle the latent space of the image to a shared content space and a domain-specific style space for unsupervised multimodal I2IT, but they have complicated network structures and multiple training losses to finetune.

In this paper, we take a fundamentally different route and design a much simpler unified model to solve the diversity problem for I2IT under both supervised and unsupervised settings. Instead of using encoders and latent code reconstruction losses like many previous methods (Zhu et al. 2017b; Lee et al. 2018; Huang et al. 2018; Almahairi et al. 2018), we propose Statistics Enhanced GAN (SEGAN) that explicitly estimates and maximizes the mutual information between the latent code and the output image by introducing

*corresponding author

†corresponding author

Preprint. Work in progress.

a statistics network into cGANs. Also, our framework only needs to learn a one-sided mapping from the source image domain to the target image domain for both supervised and unsupervised multimodal I2IT by using a U-net generator to preserve the underlying spatial information of the input image. Moreover, our method realizes the disentanglement between the source domain content and the target domain style for free. The extensive experiments demonstrate the superiority of our method.

Our contributions in this paper are summarized as follows:

- We propose SEGAN that explicitly estimates and maximizes the mutual information between the latent noise and the output image to solve the mode collapse issue in cGANs for multimodal image-to-image translation.
- By adopting a U-net generator, our SEGAN can directly learn the mapping from the source image domain to the target image domain for both supervised and unsupervised multimodal image-to-image translation.
- Our method also achieves disentanglement between the source domain content and the target domain style for free.
- We perform supervised and unsupervised image-to-image translation tasks on various benchmark datasets and compare with the state-of-the-art methods, showing the effectiveness and simplicity of our method.

Related Works

Generative adversarial networks

Generative Adversarial Networks (GANs) (Goodfellow et al. 2014) compose of two modules: a discriminator that tries to distinguish real data samples from generated samples, and a generator that tries to generate samples to fool the discriminator. There are many works proposed to improve the original GANs for more stabilized training and producing high-quality samples by better loss functions (Arjovsky, Chintala, and Bottou 2017; Zhao, Mathieu, and LeCun 2016; Berthelot, Schumm, and Metz 2017; Mao et al. 2017; Miyato et al. 2018), structure changes (Radford, Metz, and Chintala 2015; Denton et al. 2015; Karras et al. 2017; Zhang et al. 2019; Karras, Laine, and Aila 2019), or combining autoencoders (Larsen et al. 2016; Dumoulin et al. 2016; Donahue, Krähenbühl, and Darrell 2016; Che et al. 2016; Srivastava et al. 2017; Ulyanov, Vedaldi, and Lempitsky 2018). In this work, we rely on GANs to synthesize realistic images for image-to-image translation.

Image-to-image translation

Isola et al. first design a pix2pix framework based on cGANs for image-to-image translation. Then it is extended to produce high-resolution images by a coarse-to-fine way (Wang et al. 2018; Chen and Koltun 2017). But most of them need paired datasets and only produce deterministic results. For tackling the two problems, on the one hand, many works are proposed to solve the unpaired issue by semantic consistency (Taigman, Polyak, and Wolf 2016), a shared latent

space (Liu, Breuel, and Kautz 2017), pairwise sample distance (Benaim and Wolf 2017), adversarial consistency loss (Zhao, Wu, and Dong 2020), council loss (Nizan and Tal 2020), or the commonly used cycle consistency (Zhu et al. 2017a; Kim et al. 2017; Yi et al. 2017). On the other hand, for solving the diversity problem, a lot of works propose to generate multiple discrete results and encourage them to be different (Chen and Koltun 2017; Ghosh et al. 2018; Nizan and Tal 2020). For modeling continuous multimodal results, BicycleGAN (Zhu et al. 2017b) proposes to combine cVAEGAN (Larsen et al. 2016) with cLRGAN (Chen et al. 2016) to produce multimodal results under a supervised setting. Further, MUNIT (Huang et al. 2018) and DRIT (Lee et al. 2018) propose to disentangle the latent space of the image to a shared content space and a domain-specific style space for multimodal unsupervised image-to-image translation. Also, Almahairi et al. extend CycleGAN (Zhu et al. 2017a) to unsupervised many-to-many translation. In addition, Mao et al. and Yang et al. simultaneously propose a regularization that maximizes the pairwise distance between the generated images and their corresponding latent codes to encourage diversity in cGANs, which can be easily embedded in many image-to-image translation frameworks, such as pix2pix (Isola et al. 2017) and DRIT (Lee et al. 2018). Recently, Alharbi, Smith, and Wonka introduce variations for unsupervised image-to-image translation by scaling the filters of the generator. Besides, Zhao et al. propose UCTGAN that learns unsupervised cross-space translation to achieve multimodal image inpainting results. To the best of our knowledge, current state-of-the-art multimodal image-to-image translation methods are still BicycleGAN (Zhu et al. 2017b) or MSGAN (Mao et al. 2019) (which is built upon pix2pix (Isola et al. 2017)) under a supervised setting, and MUNIT (Huang et al. 2018), DRIT (Lee et al. 2018) or MSGAN (Mao et al. 2019) (which is built upon DRIT (Lee et al. 2018)) under an unsupervised setting, respectively. These methods will be put as baselines in our experiments.

Disentangled representation learning

In recent years, InfoGAN (Chen et al. 2016) and β -VAE (Higgins et al. 2016) have been proposed to learn disentangled representation for unconditional image generation. In particular, InfoGAN shares a similar idea with our method about maximizing the Mutual Information (MI). However, our method is significantly different from InfoGAN in two aspects. First, InfoGAN minimizes a variational upper bound on the conditional entropy and ignores the sample entropy of the MI, while our method explicitly estimates and maximizes the whole MI term simultaneously. Second, InfoGAN aims to learn disentangled representation for unconditional image generation, while our method focuses on the diversity of conditional image synthesis and the disentanglement between content and style in multimodal I2IT.

Mutual information

Methods based on Mutual Information (MI) can date back to the infomax principle (Linsker 1988; Bell and Sejnowski 1995), which advocates maximizing MI between the input

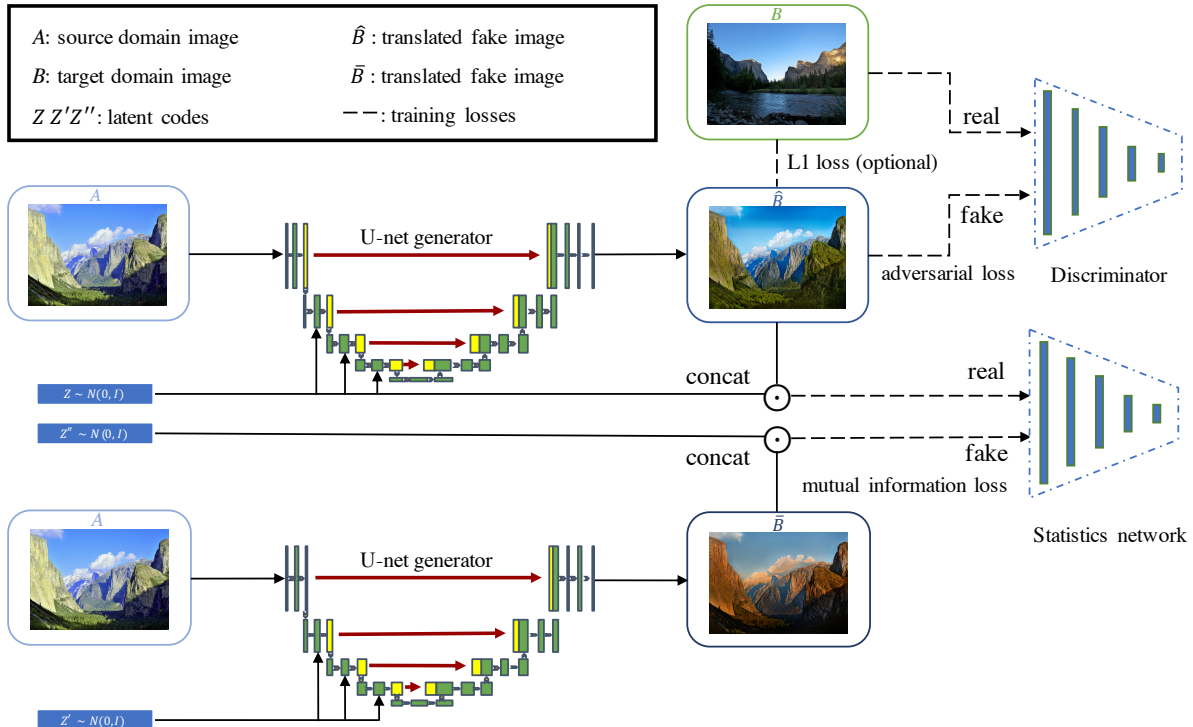


Figure 1: The network architecture and training losses of our model. Z and \hat{B} represent the correlated random variables with their realizations as the positive samples drawn from the joint distribution $p(z, \hat{b})$, and Z'' and \bar{B} are the uncorrelated random variables with their realizations as the negative samples drawn from the product of marginals $p(z)p(\hat{b})$ respectively. L1 loss only exists given paired data. Note that without the statistics network, our model is merely pix2pix+noise framework.

and output of neural networks. Some neural estimators of MI have been proposed recently, for instance, MINE (Belghazi et al. 2018) and InfoNCE (Oord, Li, and Vinyals 2018). Intuitively, these methods estimate MI between X and Y by training a classifier to distinguish between positive samples drawn from the joint distribution $p(x, y)$ and negative samples drawn from the product of marginals $p(x)p(y)$. In this work, we adopt a neural estimator similar to MINE to estimate and maximize the MI between the latent noise and the generated image in cGANs.

Method

Preliminaries

Suppose we have a source image domain $\mathcal{A} \subset \mathbb{R}^{H \times W \times C_A}$ and a target image domain $\mathcal{B} \subset \mathbb{R}^{H \times W \times C_B}$, image-to-image translation refers to learning a generator’s function $G(\cdot)$ such that $a \in \mathcal{A}$, $\hat{b} = G(a) \in \mathcal{B}$ and \hat{b} preserves some underlying spatial information of a ¹. We also refer to such underlying spatial information as “content” in this paper. In the same sense, we refer to “style” as the semantic difference of the target image domain. Under a supervised setting where paired data (a, b) are available, the adversarial loss

¹We denote the random variables with upper-case letters and their realizations with lower-case letters in this paper.

and pixel-wise loss between a and b can be combined together to learn such mapping, which is exactly the pix2pix (Isola et al. 2017) framework. To scale this framework to a multimodal case, we need to introduce latent noise Z as the source of stochasticity to the generator where the generator’s function changes to $G(a, z)$. For simplicity, the latent noise often follows an isotropic Gaussian such that $z \sim \mathcal{N}(0, I)$. We call this model pix2pix+noise. However, several works (Isola et al. 2017; Zhu et al. 2017b; Mathieu, Couprie, and LeCun 2015) have reported that naively adding the noise can hardly produce diverse results, which is also known as the issue of mode collapse of GANs (Goodfellow et al. 2014; Metz et al. 2016; Goodfellow 2016). In addition, when it comes to an unsupervised setting where no paired data (a, b) are available, the preservation of the underlying spatial information of the input image also needs to be taken into consideration. In the next, we will present our Statistics Enhanced GAN (SEGAN) framework that solves both problems.

Statistics Enhanced GAN

To solve the mode collapse problem in cGANs for multimodal image-to-image translation, we propose to strengthen the connection between the latent noise Z and the output image \hat{B} in a statistical manner, therefore we call our proposed model Statistics Enhanced GAN (SEGAN). Unlike previous

methods (Zhu et al. 2017b; Huang et al. 2018; Lee et al. 2018; Almahairi et al. 2018) that include multiple encoders and latent code reconstruction losses, SEGAN is simple and neat in its architecture. It is merely pix2pix+noise with an extension of a statistics network as shown in Fig.1. The statistics network is used to estimate the mutual information between the latent noise Z and the output image \hat{B} in cGANs. In case the latent noise Z is ignored by the generator, the generator’s function $G(a, z)$ and the conditional distribution $p(\hat{b}|a, z)$ modeled by cGANs degenerate to $G(a)$ and $p(\hat{b}|a)$ respectively, which means Z is independent of \hat{B} and the translation results become deterministic. To prevent this from happening, we explicitly estimate and maximize the Mutual Information (MI) between them. Here, the MI

$$\mathcal{I}(\hat{B}; Z) = H(\hat{B}) - H(\hat{B}|Z) = H(Z) - H(Z|\hat{B}) \quad (1)$$

quantifies the “amount of information” of \hat{B} through observing Z . To achieve diverse results, we are definitely hoping Z can affect \hat{B} in a reasonable underlying way. If Z is ignored by the generator (which means Z is independent of \hat{B}), then the MI attains its minimal value 0, because knowing Z reveals nothing about \hat{B} under such circumstances. On the contrary, if Z and \hat{B} are closely related, for example, Z is utilized by the generator to represent different styles of the target image domain, then the MI has a high value. From another perspective, the direct way to encourage the multimodality of a random variable is to maximize its entropy. As the generated sample’s entropy $H(\hat{B})$ is intractable, we use the MI between \hat{B} and Z as a proxy. As shown in Eq.1, the MI can be seen as a lower bound on $H(\hat{B})$, since $\mathcal{I}(\hat{B}; Z) = H(\hat{B}) - H(\hat{B}|Z)$.

Content-preserving effect of the U-net generator

Many previous methods use constraints like cycle consistency (Zhu et al. 2017a; Kim et al. 2017; Yi et al. 2017) to solve the unpaired problem for unsupervised I2IT. As a result, bidirectional mappings between the source image domain and the target image domain need to be learned simultaneously. However, it has been proved that only a little incentive like pairwise sample distance (Benaim and Wolf 2017) is enough for preserving the underlying spatial information of the input image. We empirically find that by using a U-net generator, which skip-connects different layers’ features of the encoder to the corresponding layers’ features of the decoder, the underlying spatial information of the input image is well-preserved with the help of the adversarial loss. We speculate it is because the encoded features of the input image from a low to a high semantic level are now highly involved in the generation process of the decoder and therefore strong connection between the input image and the translated image is built. To the best of our knowledge, we are the first to propose to use a U-net generator to preserve the underlying spatial information of the input image for unsupervised I2IT. Hence, we adopt a U-net generator in SEGAN to learn a one-sided translation model from the source image domain to the target image domain for both supervised and unsupervised multimodal image-to-image translation.

Training losses

The training losses of our framework are mainly composed of an adversarial loss and a Mutual Information (MI) loss. If paired data (a, b) are available, we also use an L1 loss in our method like many other supervised I2IT methods. The adversarial loss is used to make sure that the translated images look like real images in the target domain, while the MI loss is actually pushing the output image \hat{B} to cover the possible modes of the conditional distribution $p(\hat{b}|a, z)$.

Adversarial loss and L1 loss The adversarial loss and the L1 loss (only exists under a supervised setting) are shown as follows

$$\mathcal{L}_{\text{GAN}} = \arg \max_{D_\theta} \arg \min_{G_\gamma} \mathbb{E}_{b \sim p(b)} [\log D_\theta(b)] + \mathbb{E}_{a \sim p(a), z \sim p(z)} [\log(1 - D_\theta(G_\gamma(a, z)))] \quad (2)$$

$$\mathcal{L}_{\text{L1}} = \arg \min_{G_\gamma} \mathbb{E}_{(a,b) \sim p(a,b), z \sim p(z)} \|G_\gamma(a, z) - b\|_1 \quad (3)$$

where D , $D(\cdot)$, θ , G , $G(\cdot, \cdot)$ and γ are the discriminator, the discriminator’s critic function, the parameters of the discriminator, the generator, the generator’s function and the parameters of the generator respectively.

Mutual information loss Formally, the MI between X and Y is defined as the Kullback-Leibler (KL) divergence between the joint distribution $p(x, y)$ and the product of the marginals $p(x)p(y)$

$$\begin{aligned} \mathcal{I}(X; Y) &= D_{\text{KL}} [p(x, y) \| p(x)p(y)] \\ &= \mathbb{E}_{p(x,y)} \left[\log \frac{p(x, y)}{p(x)p(y)} \right] \end{aligned} \quad (4)$$

Belghazi et al. propose a neural estimator of the MI based on the dual formulations of the KL-divergence (Ruderman et al. 2012), such as the Donsker-Varadhan (DV) representation (Donsker and Varadhan 1983):

$$\begin{aligned} \mathcal{I}(X; Y) &:= D_{\text{KL}}(\mathbb{J} \| \mathbb{M}) \geq \hat{\mathcal{I}}^{\text{DV}}(X; Y) \\ &:= \mathbb{E}_{\mathbb{J}} [T_\omega(x, y)] - \log \mathbb{E}_{\mathbb{M}} [e^{T_\omega(x, y)}] \end{aligned} \quad (5)$$

where $T_\omega : \mathcal{X} \times \mathcal{Y} \rightarrow \mathbb{R}$ is a critic function modeled by a neural network with parameters ω , \mathbb{J} is the joint and \mathbb{M} is the product of the marginals of random variables X and Y . This estimator is trainable through back-prop and highly consistent (Belghazi et al. 2018). We switch between optimizing the statistics network T_ω to obtain the estimated MI between Z and \hat{B} and maximizing their MI w.r.t. the generator’s parameters γ during training, which is similar to the adversarial training between D and G in GANs. The MI loss is defined as

$$\mathcal{L}_{\text{MI}} = \arg \max_{T_\omega} \arg \max_{G_\gamma} \hat{\mathcal{I}}_\omega(Z; G_\gamma(\cdot, Z)) \quad (6)$$

where $\hat{\mathcal{I}}_\omega$ denotes the MI estimator parameterized by ω .

However, the DV MI estimator which is based on the KL divergence between the joint and the products of the marginals of the random variables has some problems such as biased estimate of the batch gradient and unbounded value (Belghazi et al. 2018). And as our goal is to maximize the MI, not concerned about its precise value, we adopt a Jensen-Shannon Divergence (JSD) MI estimator (following the formulation of f-gan (Nowozin, Cseke, and Tomioka 2016), refer to the Appendix for more details about the relation between the MI and the JSD MI estimator). A similar estimator is also used in DeepInfoMax (Hjelm et al. 2018) for unsupervised representation learning. The JSD MI estimator is defined as

$$\begin{aligned} \text{JSD} \left(p(z, \hat{b}) \| p(z)p(\hat{b}) \right) &\geq \\ \hat{T}_\omega^{JSD}(Z; G_\gamma(\cdot, Z)) &= \mathbb{E}_{p_z} [-\text{sp}(-T_\omega(z, G_\gamma(\cdot, z)))] - \\ &\quad \mathbb{E}_{\hat{p}_z \times \bar{p}_z} [\text{sp}(T_\omega(z'', G_\gamma(\cdot, z'')))] \end{aligned} \quad (7)$$

where $p_z = \hat{p}_z = \bar{p}_z = \mathcal{N}(0, I)$, z' and z'' are the samples from \hat{p}_z and \bar{p}_z respectively, and $\text{sp}(x) = \log(1 + e^x)$ is the softplus function. The mathematical form of the JSD MI estimator amounts to the familiar binary cross-entropy, which has been well-developed as the loss function for binary classification through neural networks. Besides, we find the JSD MI estimator is more stable during training than the DV MI estimator. We treat the correlated samples $(z, \hat{b} = G(\cdot, z))$ drawn from the joint distribution $p(z, \hat{b})$ as the positive samples and the uncorrelated samples $(z'', \bar{b} = G(\cdot, z''))$ drawn from the product of marginals $p(z)p(\bar{b})$ as the negative samples respectively as shown in Fig.1. The final objective function of our model is shown as follows (L1 loss only exists under a supervised setting)

$$\mathcal{L} = \mathcal{L}_{\text{GAN}} + \lambda_1 \mathcal{L}_{\text{MI}} + \lambda_2 \mathcal{L}_{\text{L1}} \quad (8)$$

where λ_1 and λ_2 are the weights controlling the importance of the corresponding losses.

Disentanglement between content and style

Since the Mutual Information (MI) between the latent noise Z and the output image $\hat{B} = G(\cdot, Z)$ is maximized regardless of the input image A as shown in Eq.6 (which means we randomly sample different $a \sim p(a)$ to combine with the same $z \sim p(z)$ to form the positive samples $(z, G(a, z))$ during training), the latent noise affects the output image in a global way and disentangles from the input A . And as the preservation of the content of the input image is ensured by our U-net generator design, we achieve disentanglement between the source domain content A and the target domain style Z for free. Therefore, unlike previous methods (Huang et al. 2018; Lee et al. 2018) which explicitly disentangle the latent space of the image to a shared content space and a domain-specific style space, our model realizes such disentanglement for free as a result of the MI maximization.

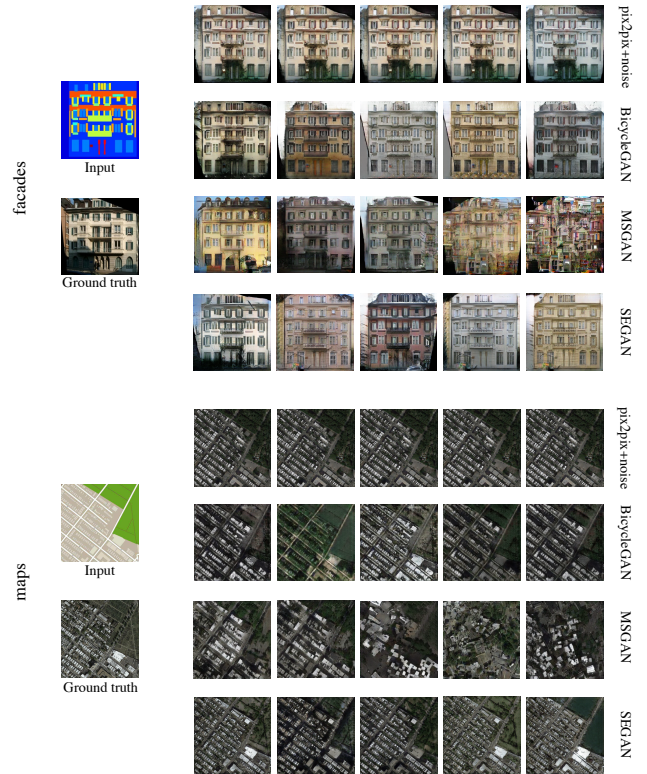


Figure 2: The qualitative results on facades and maps datasets. Our method achieves both diverse and high-quality results. Zoom in to see more details.

Experiments

Datasets & baselines

We evaluate our model on facades and maps (Zhu et al. 2017b) datasets under a supervised setting, and on edges2shoes (Yu and Grauman 2014; Zhu et al. 2016), Yosemite winter2summer (Zhu et al. 2017a) and cat2dog (Lee et al. 2018) datasets under an unsupervised setting. Note that we train our model on edges2shoes dataset without supervision, but we also compare with BicycleGAN on this dataset which is trained given paired information. Unlike MUNIT and DRIT, we only train a one-sided translation model from the source image domain to the target image domain for unsupervised multimodal I2IT.

We compare our method with several state-of-the-art methods for multimodal I2IT, such as BicycleGAN (Zhu et al. 2017b), MSGAN (Mao et al. 2019), MUNIT (Huang et al. 2018) and DRIT (Lee et al. 2018).

methods	facades		maps	
	LPIPS \uparrow	FID \downarrow	LPIPS \uparrow	FID \downarrow
MSGAN	0.189	92.84 \pm 1.00	0.219	152.46 \pm 2.52
BicycleGAN	0.144	98.85 \pm 1.21	0.115	145.78 \pm 3.90
SEGAN (ours)	0.156	82.57 \pm 0.32	0.130	114.11 \pm 2.29

Table 1: Quantitative results of different methods on facades and maps datasets under a supervised setting.

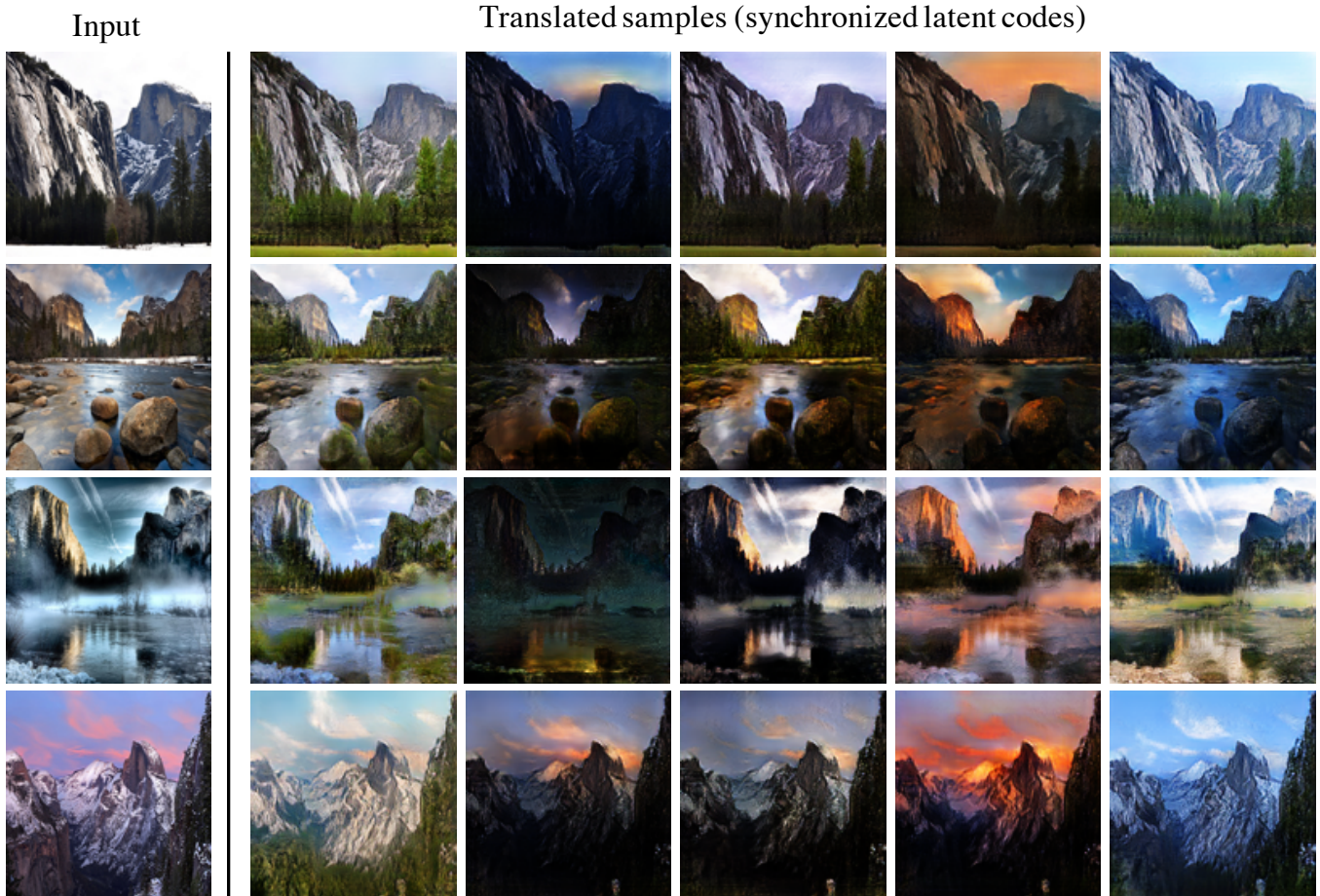


Figure 3: The qualitative results of our method on Yosemite winter2summer dataset. Each column’s images are produced by the same latent code.

Evaluation metrics

We follow the settings of previous methods (Zhu et al. 2017b; Huang et al. 2018; Lee et al. 2018; Mao et al. 2019) and mainly use three metrics for quantitative evaluation: FID (Heusel et al. 2017), LPIPS (Zhang et al. 2018) and user study. FID measures the quality and the diversity of the generated images by calculating the distance between the model distribution and the real one through deep features. LPIPS measures the average feature distances between generated samples which can reflect the diversity. User study reports the likelihood of images generated by our method to be preferred over another method. For LPIPS and user study, the higher the better, but the opposite for FID. More evaluation details can be found in the Appendix.

We also present the translated samples of different methods for qualitative comparison. More qualitative results of our method can be found in the Appendix.

Supervised results

We conduct experiments on facades and maps datasets under a supervised setting and compare with BicycleGAN (Zhu et al. 2017b) and MSGAN (Mao et al. 2019). For fair com-

parison, all methods use the same network architecture. The translated samples of these methods are depicted in Fig.2. We can find that pix2pix+noise is prone to run into mode collapse, while SEGAN can produce both diverse and high-quality results. The quantitative results on these datasets are shown in Tab.1. Despite much higher LPIPS scores obtained by MSGAN than ours, we find it often produces collapsed samples with a lot of artifacts as shown in the rightmost images of MSGAN in Fig.2. This phenomenon is much worse on maps dataset and it may cause the much higher LPIPS scores of MSGAN on both datasets. It is also verified by the FID in Tab.1 as our method beats MSGAN with a large margin. Also, our method is superior to BicycleGAN in both LPIPS and FID as shown in Tab.1.

Unsupervised results

We present our experimental results on edges2shoes, Yosemite winter2summer and cat2dog datasets under an unsupervised setting. We do not use any content-preserving constraints like cycle consistency (Zhu et al. 2017a; Kim et al. 2017; Yi et al. 2017) and only rely on a U-net generator to preserve the underlying spatial information of the input



Figure 4: The qualitative results on edges2shoes and cat2dog datasets. In the middle, we show the translated samples produced by the same latent code on edges2shoes dataset by our method.

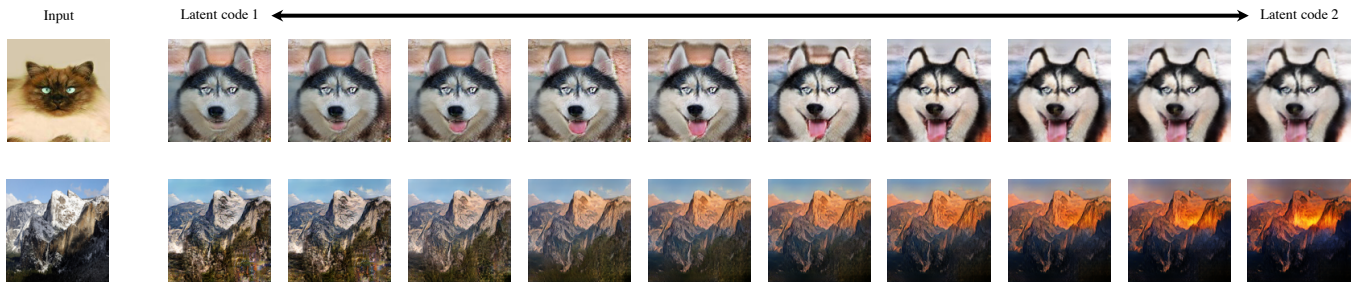


Figure 5: The results of latent space interpolation on cat2dog and Yosemite winter2summer datasets.

methods	edges2shoes		winter2summer	
	User study \uparrow	LPIPS \uparrow	User study \uparrow	LPIPS \uparrow
MUNIT	46.4%	0.109	58.3%	0.091
DRIT	N/A	N/A	55.6%	0.097
MSGAN	N/A	N/A	58.8%	0.118
BicycleGAN	43.6%	0.144	N/A	N/A
SEGAN (ours)	N/A	0.156	N/A	0.170

Table 2: Quantitative results of different methods on edges2shoes and winter2summer datasets under an unsupervised setting. Note that BicycleGAN is trained with supervision on edges2shoes dataset.

image. The translated samples on Yosemite winter2summer, and edges2shoes and cat2dog datasets are shown in Fig.3 and Fig.4 respectively. The sources of variations learned by our model on Yosemite winter2summer dataset include the light, the amount of clouds and the luxuriance of vegetation as shown in Fig.3. Also, our method generates diverse and high-quality samples on edges2shoes dataset as shown in Fig.4. Moreover, we can clearly see that even on the shape-variant dataset like cat2dog, the underlying spatial information (which is pose in this case) is well preserved by our method in Fig.4. The quantitative results on edges2shoes and winter2summer datasets are depicted in Tab.2, which shows that our method achieves comparable quality and higher diversity against state-of-the-art methods.

Interpolation of latent space

We also perform linear interpolation between two given latent codes and generate corresponding images to show the generalization of our model to capture the full conditional distribution. We perform the interpolation experiments on cat2dog and Yosemite winter2summer datasets. We can find that the interpolation in latent space results in smooth changes in semantic level as shown in Fig.5.

Disentanglement between content and style

To show our model achieves the disentanglement between the source domain content and the target domain style for free. We show the samples generated from the synchronized latent codes on different input images on Yosemite winter2summer and edges2shoes datasets in Fig.3 and Fig.4 respectively. We can find that the latent code which controls the styles of the target image domain disentangles well from the source domain content.

Conclusion

In this paper, we present a novel model SEGAN that can achieve diverse and high-quality results for both supervised and unsupervised multimodal image-to-image translation. Future work includes extending SEGAN to other diverse conditional image synthesis tasks such as image inpainting and style transfer.

References

- Alharbi, Y.; Smith, N.; and Wonka, P. 2019. Latent filter scaling for multimodal unsupervised image-to-image translation. In *Proceedings of the IEEE Conference on Computer Vision and Pattern Recognition*, 1458–1466.
- Almahairi, A.; Rajeswar, S.; Sordoni, A.; Bachman, P.; and Courville, A. 2018. Augmented cyclegan: Learning many-to-many mappings from unpaired data. *arXiv preprint arXiv:1802.10151*.
- Arjovsky, M.; Chintala, S.; and Bottou, L. 2017. Wasserstein gan. *arXiv preprint arXiv:1701.07875*.
- Belghazi, M. I.; Baratin, A.; Rajeswar, S.; Ozair, S.; Bengio, Y.; Courville, A.; and Hjelm, R. D. 2018. Mine: mutual information neural estimation. *arXiv preprint arXiv:1801.04062*.
- Bell, A. J.; and Sejnowski, T. J. 1995. An information-maximization approach to blind separation and blind deconvolution. *Neural computation* 7(6): 1129–1159.
- Benaïm, S.; and Wolf, L. 2017. One-sided unsupervised domain mapping. In *Advances in neural information processing systems*, 752–762.
- Berthelot, D.; Schumm, T.; and Metz, L. 2017. Began: Boundary equilibrium generative adversarial networks. *arXiv preprint arXiv:1703.10717*.
- Che, T.; Li, Y.; Jacob, A. P.; Bengio, Y.; and Li, W. 2016. Mode regularized generative adversarial networks. *arXiv preprint arXiv:1612.02136*.
- Chen, Q.; and Koltun, V. 2017. Photographic image synthesis with cascaded refinement networks. In *Proceedings of the IEEE international conference on computer vision*, 1511–1520.
- Chen, X.; Duan, Y.; Houthoofd, R.; Schulman, J.; Sutskever, I.; and Abbeel, P. 2016. Infogan: Interpretable representation learning by information maximizing generative adversarial nets. In *Advances in neural information processing systems*, 2172–2180.
- Denton, E.; Chintala, S.; Szlam, A.; and Fergus, R. 2015. Deep Generative Image Models using a Laplacian Pyramid of Adversarial Networks. *arXiv preprint arXiv:1506.05751*.
- Donahue, J.; Krähenbühl, P.; and Darrell, T. 2016. Adversarial feature learning. *arXiv preprint arXiv:1605.09782*.
- Donsker, M. D.; and Varadhan, S. S. 1983. Asymptotic evaluation of certain Markov process expectations for large time. IV. *Communications on Pure and Applied Mathematics* 36(2): 183–212.
- Dumoulin, V.; Belghazi, I.; Poole, B.; Mastropietro, O.; Lamb, A.; Arjovsky, M.; and Courville, A. 2016. Adversarially learned inference. *arXiv preprint arXiv:1606.00704*.
- Gatys, L. A.; Ecker, A. S.; and Bethge, M. 2016. Image style transfer using convolutional neural networks. In *Proceedings of the IEEE conference on computer vision and pattern recognition*, 2414–2423.
- Ghosh, A.; Kulharia, V.; Namboodiri, V. P.; Torr, P. H.; and Dokania, P. K. 2018. Multi-agent diverse generative adversarial networks. In *Proceedings of the IEEE conference on computer vision and pattern recognition*, 8513–8521.
- Goodfellow, I. 2016. NIPS 2016 tutorial: Generative adversarial networks. *arXiv preprint arXiv:1701.00160*.
- Goodfellow, I.; Pouget-Abadie, J.; Mirza, M.; Xu, B.; Warde-Farley, D.; Ozair, S.; Courville, A.; and Bengio, Y. 2014. Generative adversarial nets. In *Advances in neural information processing systems*, 2672–2680.
- Heusel, M.; Ramsauer, H.; Unterthiner, T.; Nessler, B.; and Hochreiter, S. 2017. Gans trained by a two time-scale update rule converge to a local nash equilibrium. In *Advances in neural information processing systems*, 6626–6637.
- Higgins, I.; Matthey, L.; Pal, A.; Burgess, C.; Glorot, X.; Botvinick, M.; Mohamed, S.; and Lerchner, A. 2016. beta-vae: Learning basic visual concepts with a constrained variational framework.
- Hjelm, R. D.; Fedorov, A.; Lavoie-Marchildon, S.; Grewal, K.; Bachman, P.; Trischler, A.; and Bengio, Y. 2018. Learning deep representations by mutual information estimation and maximization. *arXiv preprint arXiv:1808.06670*.
- Huang, X.; Liu, M.-Y.; Belongie, S.; and Kautz, J. 2018. Multimodal unsupervised image-to-image translation. In *Proceedings of the European Conference on Computer Vision (ECCV)*, 172–189.
- Isola, P.; Zhu, J.-Y.; Zhou, T.; and Efros, A. A. 2017. Image-to-image translation with conditional adversarial networks. In *Proceedings of the IEEE conference on computer vision and pattern recognition*, 1125–1134.
- Karras, T.; Aila, T.; Laine, S.; and Lehtinen, J. 2017. Progressive growing of gans for improved quality, stability, and variation. *arXiv preprint arXiv:1710.10196*.
- Karras, T.; Laine, S.; and Aila, T. 2019. A style-based generator architecture for generative adversarial networks. In *Proceedings of the IEEE conference on computer vision and pattern recognition*, 4401–4410.
- Kim, T.; Cha, M.; Kim, H.; Lee, J. K.; and Kim, J. 2017. Learning to discover cross-domain relations with generative adversarial networks. *arXiv preprint arXiv:1703.05192*.
- Larsen, A. B. L.; Sønderby, S. K.; Larochelle, H.; and Winther, O. 2016. Autoencoding beyond pixels using a learned similarity metric. In *International conference on machine learning*, 1558–1566.
- Ledig, C.; Theis, L.; Huszár, F.; Caballero, J.; Cunningham, A.; Acosta, A.; Aitken, A.; Tejani, A.; Totz, J.; Wang, Z.; et al. 2017. Photo-realistic single image super-resolution using a generative adversarial network. In *Proceedings of the IEEE conference on computer vision and pattern recognition*, 4681–4690.
- Lee, H.-Y.; Tseng, H.-Y.; Huang, J.-B.; Singh, M.; and Yang, M.-H. 2018. Diverse image-to-image translation via disentangled representations. In *Proceedings of the European conference on computer vision (ECCV)*, 35–51.

- Linsker, R. 1988. Self-organization in a perceptual network. *Computer* 21(3): 105–117.
- Liu, M.-Y.; Breuel, T.; and Kautz, J. 2017. Unsupervised image-to-image translation networks. In *Advances in neural information processing systems*, 700–708.
- Mao, Q.; Lee, H.-Y.; Tseng, H.-Y.; Ma, S.; and Yang, M.-H. 2019. Mode seeking generative adversarial networks for diverse image synthesis. In *Proceedings of the IEEE Conference on Computer Vision and Pattern Recognition*, 1429–1437.
- Mao, X.; Li, Q.; Xie, H.; Lau, R. Y.; Wang, Z.; and Paul Smolley, S. 2017. Least squares generative adversarial networks. In *Proceedings of the IEEE international conference on computer vision*, 2794–2802.
- Mathieu, M.; Couprie, C.; and LeCun, Y. 2015. Deep multi-scale video prediction beyond mean square error. *arXiv preprint arXiv:1511.05440*.
- Metz, L.; Poole, B.; Pfau, D.; and Sohl-Dickstein, J. 2016. Unrolled generative adversarial networks. *arXiv preprint arXiv:1611.02163*.
- Mirza, M.; and Osindero, S. 2014. Conditional generative adversarial nets. *arXiv preprint arXiv:1411.1784*.
- Miyato, T.; Kataoka, T.; Koyama, M.; and Yoshida, Y. 2018. Spectral normalization for generative adversarial networks. *arXiv preprint arXiv:1802.05957*.
- Nizan, O.; and Tal, A. 2020. Breaking the Cycle-Colleagues Are All You Need. In *Proceedings of the IEEE/CVF Conference on Computer Vision and Pattern Recognition*, 7860–7869.
- Nowozin, S.; Cseke, B.; and Tomioka, R. 2016. f-gan: Training generative neural samplers using variational divergence minimization. In *Advances in neural information processing systems*, 271–279.
- Oord, A. v. d.; Li, Y.; and Vinyals, O. 2018. Representation learning with contrastive predictive coding. *arXiv preprint arXiv:1807.03748*.
- Pathak, D.; Krahenbuhl, P.; Donahue, J.; Darrell, T.; and Efros, A. A. 2016. Context encoders: Feature learning by inpainting. In *Proceedings of the IEEE conference on computer vision and pattern recognition*, 2536–2544.
- Radford, A.; Metz, L.; and Chintala, S. 2015. Unsupervised representation learning with deep convolutional generative adversarial networks. *arXiv preprint arXiv:1511.06434*.
- Ruderman, A.; Reid, M.; García-García, D.; and Petterson, J. 2012. Tighter variational representations of f-divergences via restriction to probability measures. *arXiv preprint arXiv:1206.4664*.
- Srivastava, A.; Valkov, L.; Russell, C.; Gutmann, M. U.; and Sutton, C. 2017. Veegan: Reducing mode collapse in gans using implicit variational learning. In *Advances in Neural Information Processing Systems*, 3308–3318.
- Taigman, Y.; Polyak, A.; and Wolf, L. 2016. Unsupervised cross-domain image generation. *arXiv preprint arXiv:1611.02200*.
- Ulyanov, D.; Vedaldi, A.; and Lempitsky, V. 2018. It takes (only) two: Adversarial generator-encoder networks. In *Thirty-Second AAAI Conference on Artificial Intelligence*.
- Wang, T.-C.; Liu, M.-Y.; Zhu, J.-Y.; Tao, A.; Kautz, J.; and Catanzaro, B. 2018. High-resolution image synthesis and semantic manipulation with conditional gans. In *Proceedings of the IEEE conference on computer vision and pattern recognition*, 8798–8807.
- Yang, D.; Hong, S.; Jang, Y.; Zhao, T.; and Lee, H. 2019. Diversity-sensitive conditional generative adversarial networks. *arXiv preprint arXiv:1901.09024*.
- Yi, Z.; Zhang, H.; Tan, P.; and Gong, M. 2017. Dualgan: Unsupervised dual learning for image-to-image translation. In *Proceedings of the IEEE international conference on computer vision*, 2849–2857.
- Yu, A.; and Grauman, K. 2014. Fine-grained visual comparisons with local learning. In *Proceedings of the IEEE Conference on Computer Vision and Pattern Recognition*, 192–199.
- Zhang, H.; Goodfellow, I.; Metaxas, D.; and Odena, A. 2019. Self-attention generative adversarial networks. In *International Conference on Machine Learning*, 7354–7363.
- Zhang, H.; Xu, T.; Li, H.; Zhang, S.; Wang, X.; Huang, X.; and Metaxas, D. N. 2017. Stackgan: Text to photo-realistic image synthesis with stacked generative adversarial networks. In *Proceedings of the IEEE international conference on computer vision*, 5907–5915.
- Zhang, R.; Isola, P.; Efros, A. A.; Shechtman, E.; and Wang, O. 2018. The unreasonable effectiveness of deep features as a perceptual metric. In *Proceedings of the IEEE conference on computer vision and pattern recognition*, 586–595.
- Zhao, J.; Mathieu, M.; and LeCun, Y. 2016. Energy-based generative adversarial network. *arXiv preprint arXiv:1609.03126*.
- Zhao, L.; Mo, Q.; Lin, S.; Wang, Z.; Zuo, Z.; Chen, H.; Xing, W.; and Lu, D. 2020. UCTGAN: Diverse Image Inpainting Based on Unsupervised Cross-Space Translation. In *Proceedings of the IEEE/CVF Conference on Computer Vision and Pattern Recognition*, 5741–5750.
- Zhao, Y.; Wu, R.; and Dong, H. 2020. Unpaired Image-to-Image Translation using Adversarial Consistency Loss. *arXiv preprint arXiv:2003.04858*.
- Zhu, J.-Y.; Krähenbühl, P.; Shechtman, E.; and Efros, A. A. 2016. Generative visual manipulation on the natural image manifold. In *European conference on computer vision*, 597–613. Springer.
- Zhu, J.-Y.; Park, T.; Isola, P.; and Efros, A. A. 2017a. Unpaired image-to-image translation using cycle-consistent adversarial networks. In *Proceedings of the IEEE international conference on computer vision*, 2223–2232.
- Zhu, J.-Y.; Zhang, R.; Pathak, D.; Darrell, T.; Efros, A. A.; Wang, O.; and Shechtman, E. 2017b. Toward multimodal image-to-image translation. In *Advances in neural information processing systems*, 465–476.

The Jensen-Shannon Divergence Mutual Information estimator

We show that positive correlation exists between the Mutual Information (MI) and the Jensen-Shannon Divergence (JSD) MI estimator. They are related by Pointwise Mutual Information (PMI)

$$\text{PMI}(x; y) \equiv \log \frac{p(x, y)}{p(x)p(y)} = \log \frac{p(y|x)}{p(y)} \quad (9)$$

$$\begin{aligned} \text{MI} \equiv \mathcal{I}(X; Y) &= D_{\text{KL}}[p(x, y) \| p(x)p(y)] \\ &= \mathbb{E}_{p(x, y)} \left[\log \frac{p(x, y)}{p(x)p(y)} \right] \\ &= \mathbb{E}_{p(x, y)} [\text{PMI}(x; y)] \end{aligned} \quad (10)$$

Derivation from (Hjelm et al. 2018), we have

$$\begin{aligned} \text{JSD}(p(x, y) \| p(x)p(y)) &\propto \\ \mathbb{E}_{p(x, y)} \left[\log \frac{p(y|x)}{p(y)} - \left(1 + \frac{p(y)}{p(y|x)} \right) \log \left(1 + \frac{p(y|x)}{p(y)} \right) \right] \end{aligned} \quad (11)$$

The quantity inside the expectation of Eq.11 is a concave, monotonically increasing function of the ratio $\frac{p(y|x)}{p(y)}$, which is $e^{\text{PMI}(x, y)}$. Therefore, positive correlation exists between the MI and the JSD MI estimator.

Training details

We set $\lambda_1 = 1$ in all our experiments and $\lambda_2 = 3$ under a supervised setting. We use a U-net generator and a multi-scale patch discriminator similar to (Isola et al. 2017) in our framework. We use a latent code dimension of 8 in all our experiments. The noise is replicated to form 8 feature channels and concatenate with other features in every layer of the U-net generator’s encoder like BicycleGAN (Zhu et al. 2017b). The statistics network in our framework is a Convolutional Neural Network (CNN) with a few layers of MLP (Multilayer Perceptron) which takes the latent noise as input. For estimating the MI by using Monte Carlo sampling, we need a reasonable sample size to avoid large variance, therefore we use a batch size of 32 for the neural estimator (a batch size of 4 for input images and 8 translated images per input image). We empirically find that increasing the sample size leads to more diverse results even without the mutual information loss. We also find that excluding the positive samples from the products of marginals and increasing the ratio of the negative samples to the positive samples may help stabilize training. We use RTX2080 8G for our experiments and implement our model with PyTorch v1.2.0 on ArchLinux. Due to the memory limitation of the GPU that we use, we train on facades and maps dataset with image size 256×256 and deconv upsampling layers and on other datasets with image size 128×128 and resize-conv upsampling layers respectively. We show the architectures of the statistics network for image size 256×256 and 128×128 in Tab.3 and Tab.4 respectively.

Convolutional Neural Network	Multilayer Perceptron
Input 256×256	Input latent code with a dimension of 8
4×4 conv. 32 ELU, stride 2	N/A
4×4 conv. 64 ELU, stride 2	N/A
4×4 conv. 128 ELU, stride 2	N/A
4×4 conv. 256 ELU, stride 2	N/A
4×4 conv. 512 ELU, stride 2	N/A
4×4 conv. 1024 ELU, stride 2	FC. 512 ELU
FC. 1024 ELU	FC. 1024 ELU
FC. 1 none (add the previous layers together)	

Table 3: The statistics network’s architecture for image size 256×256 .

Convolutional Neural Network	Multilayer Perceptron
Input 128×128	Input latent code with a dimension of 8
4×4 conv. 32 ELU, stride 2	N/A
4×4 conv. 64 ELU, stride 2	N/A
4×4 conv. 128 ELU, stride 2	N/A
4×4 conv. 256 ELU, stride 2	N/A
4×4 conv. 512 ELU, stride 2	FC. 512 ELU
FC. 1024 ELU	FC. 1024 ELU
FC. 1 none (add the previous layers together)	

Table 4: The statistics network’s architecture for image size 128×128 .

Evaluation details

For the FID, similar to (Mao et al. 2019), we randomly generate 50 images per input image in the test set. We randomly choose 100 input images and their corresponding generated images to form 5000 generated samples. We use the 5000 generated samples and all samples in training set to compute FID. The FID results is averaged over 5 runs. For fair comparison, as our method shares the same network architecture and generated image size with BicycleGAN (Zhu et al. 2017b) and MSGAN (Mao et al. 2019) on supervised experiments, we only report FID on these experiments.

For the LPIPS distance, we follow the settings from (Zhu et al. 2017b). We use 100 input images from the test set and sample 20 translated images for each input image. Then we compute all possible pairs of the images sampled from the same image and average over them on 100 input images.

For the user study, similar to (Huang et al. 2018; Wang et al. 2018), the workers are given an input image and two translated images from different methods. They are then given unlimited time to select which translated sample looks accurate and has higher quality. For each comparison, we randomly generate 100 questions and each question is answered by 5 different individuals.

The content-preserving effect of the U-net generator

We show SEGAN’s translated results by using different network structures of the generator in Fig.6. One is the resnet generator which is composed of a few downsampling and upsampling layers and several residual blocks (Huang et al. 2018) and the other is the U-net generator. We can clearly find that the resnet generator fails to preserve the spatial information of the input image, while the U-net generator pre-

serves the spatial information of the input image well.

More qualitative results

Here we display more qualitative results of our method on the Yosemite winter2summer, cat2dog, edges2shoes, facades and maps datasets on Fig.7, Fig.8, Fig.9, Fig.10 and Fig.11 respectively. All the translated samples are produced by synchronized latent codes on different input images.

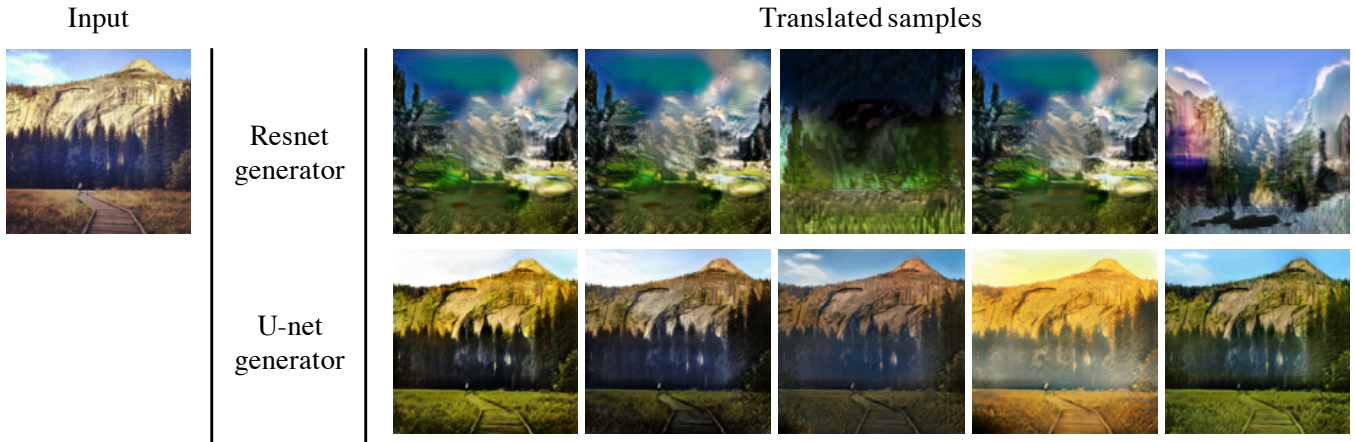


Figure 6: Different results of SEGAN by using the resnet generator and the U-net generator on Yosemite winter2summer dataset.



Figure 7: More qualitative results of our method on Yosemite winter2summer dataset.

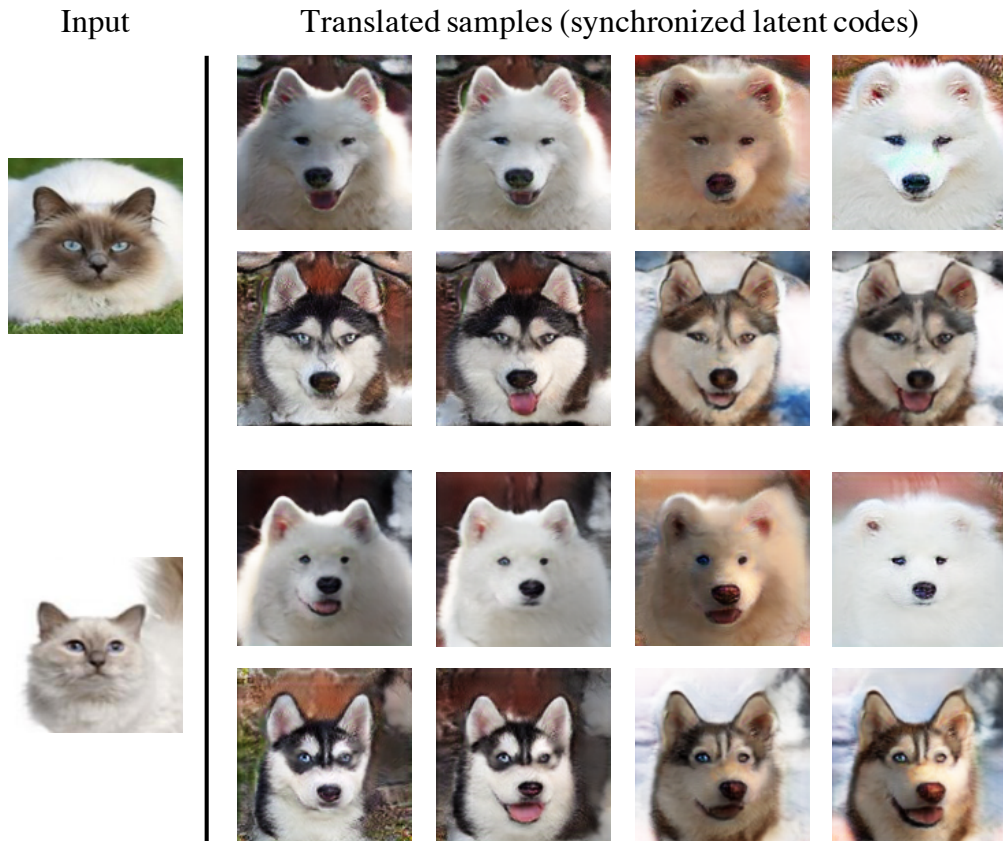


Figure 8: More qualitative results of our method on cat2dog dataset.



Figure 9: More qualitative results of our method on edges2shoes dataset.



Figure 10: More qualitative results of our method on facades dataset.



Figure 11: More qualitative results of our method on maps dataset.